Genome and Epigenome

Cancer Research

Network Modeling of microRNA–mRNA Interactions in Neuroblastoma Tumorigenesis Identifies miR-204 as a Direct Inhibitor of MYCN

Chi Yan Ooi[1], Daniel R. Carter[1,2], Bing Liu[1], Chelsea Mayoh[1], Anneleen Beckers[3], Amit Lalwani[1], Zsuzsanna Nagy[1], Sara De Brouwer[3], Bieke Decaesteker[3], Tzong-Tyng Hung[4], Murray D. Norris[1,5], Michelle Haber[1], Tao Liu[1], Katleen De Preter[3], Frank Speleman[3], Belamy B. Cheung[1,2], and Glenn M. Marshall[1,2,6]

Abstract

Neuroblastoma is a pediatric cancer of the sympathetic nervous system where *MYCN* amplification is a key indicator of poor prognosis. However, mechanisms by which MYCN promotes neuroblastoma tumorigenesis are not fully understood. In this study, we analyzed global miRNA and mRNA expression profiles of tissues at different stages of tumorigenesis from TH-MYCN transgenic mice, a model of MYCN-driven neuroblastoma. On the basis of a Bayesian learning network model in which we compared pretumor ganglia from TH-MYCN$^{+/+}$ mice to age-matched wild-type controls, we devised a predicted miRNA–mRNA interaction network. Among the miRNA–mRNA interactions operating during human neuroblastoma tumorigenesis, we identified miR-204 as a tumor suppressor miRNA that inhibited a subnetwork of oncogenes strongly associated with *MYCN*-amplified neuroblastoma and poor patient outcome. MYCN bound to the miR-204 promoter and repressed miR-204 transcription. Conversely, miR-204 directly bound MYCN mRNA and repressed MYCN expression. miR-204 overexpression significantly inhibited neuroblastoma cell proliferation *in vitro* and tumorigenesis *in vivo*. Together, these findings identify novel tumorigenic miRNA gene networks and miR-204 as a tumor suppressor that regulates MYCN expression in neuroblastoma tumorigenesis.

Significance: Network modeling of miRNA–mRNA regulatory interactions in a mouse model of neuroblastoma identifies miR-204 as a tumor suppressor and negative regulator of MYCN.
Cancer Res; 78(12); 3122–34. ©2018 AACR.

Introduction

Neuroblastoma is a pediatric malignancy that derives from the progenitors of the sympathetic nervous system (1). Despite being relatively rare, neuroblastoma accounts for approximately 15% of pediatric cancer–related deaths, mostly attributed to patients with high-stage disease who relapse despite intensive multimodal therapy (2). *MYCN* amplification is one of the strongest clinical predictors of poor prognosis, but targeted therapies for patients with *MYCN*-amplified disease remain elusive (2). The role of MYCN as a driver of neuroblastoma is well established, as TH-MYCN mice develop neuroblastoma highly similar to the human disease and have been used extensively to model mechanisms of tumor initiation (3, 4).

Tumors in TH-MYCN mice develop in 100% of homozygote (+/+) mice by 6–7 weeks of age and 25% of hemizygote (+/−) mice by 12–13 weeks of age (4, 5). Tumors mostly form in the abdomen, commonly as part of the sympathetic ganglia in this region, but similar to the human disease, tumors also occur in sympathetic ganglia of the chest and neck in some occasions. Tumor initiation in TH-MYCN mice is characterized by premalignant hyperplasia of neuroblast progenitors in sympathetic ganglia, followed by clonal selection of a minor population of tumor-initiating cells that develop into neuroblastoma (5). Contributing mechanisms to this process have been observed, including dysfunctional neural crest development, disturbances of apoptotic activation, metabolic deregulation, and oncogenic activation of MYCN-regulatory targets (6–13).

It is now clear that noncoding RNAs have important functional roles in regulation of normal cellular homeostasis and disease (14). Noncoding RNAs have multiple regulatory functions in cancer including regulation of mRNA stability and translation, genomic stability, transcriptional regulation, and epigenetic modifications (14). The most well-studied group of noncoding RNAs are miRNAs, which are closely linked to regulation of mRNA

[1]Children's Cancer Institute Australia, Lowy Cancer Research Centre, University of New South Wales, Randwick, New South Wales, Australia. [2]School of Women's & Children's Health, University of New South Wales Australia, Randwick, New South Wales, Australia. [3]Center for Medical Genetics (CMGG), Ghent University, Medical Research Building (MRB1), Ghent, Belgium. [4]Biological Resource Imaging Laboratory, the University of New South Wales, Kensington, New South Wales, Australia. [5]Centre for Childhood Cancer Research, University of New South Wales, Randwick, New South Wales, Australia. [6]Kids Cancer Centre, Sydney Children's Hospital, Randwick, New South Wales, Australia.

Note: Supplementary data for this article are available at Cancer Research Online (http://cancerres.aacrjournals.org/).

C.Y. Ooi and D.R. Carter are the co-first authors of this article.

Corresponding Authors: Belamy B. Cheung, Children's Cancer Institute Australia, Lowy Cancer Research Centre, University of New South Wales, Randwick 2031, Australia. Phone: 612-9385-2450; Fax: 612-9662-6583; E-mail: BCheung@ccia.org.au; and Glenn M Marshall, Children's Cancer Institute Australia, Lowy Cancer Research Centre, University of New South Wales, Randwick 2031, Australia. Phone: 612-9385-2516; E-mail: g.marshall@unsw.edu.au

doi: 10.1158/0008-5472.CAN-17-3034

stability/translation in multiple cancers (14, 15). Numerous reports have identified that miRNAs regulate neuroblastoma tumorigenesis, progression, and prognosis (8, 16–18). MYCN and closely related MYC, which are frequently deregulated in neuroblastoma and other cancers, also participate in miRNA regulatory networks. Notable regulatory links between MYC proteins and miRNAs include oncogenic miRNAs such as those from the miR-17–92 cluster, and tumor suppressor miRNAs, such as the let-7 family and miR-34 (7, 8, 19, 20). The functional relevance of miRNA–mRNA networks in MYCN-driven neuroblastoma tumorigenesis is still poorly understood.

In this study, we used gene expression data from TH-MYCN mice to create a predicted miRNA–mRNA interaction network. We describe a number of novel interactions and cross-validate these predictions in human neuroblastoma samples. We focus on the novel relationship between miR-204 and MYCN and its relevance to neuroblastoma tumorigenesis.

Materials and Methods

Neuroblastoma cell models

Cells were sourced as follows: BE(2)C, SH-SY5Y, and SHEP (gift from Dr. J Biedler, Memorial Sloan Kettering Cancer Center, New York, NY), Kelly, SK-N-AS and SK-N-FI (European Collection of Cell Cultures), IMR32 (purchased from ATCC). Media for maintenance of cells was as follows: BE(2)C and Kelly (RPMI1640 + 10% FCS), SK-N-AS, SK-N-FI, SH-SY5Y, SHEP, and IMR32 (DMEM + 10% FCS). All cell lines were authenticated using short-tandem repeat DNA profiling at Cell Bank Australia between 2011 and 2013 and were mycoplasma free. Cells were maintained in logarithmic growth phase in a humidified atmosphere containing 5% CO_2 at 37°C, passaged every 2–3 days by trypsinization.

Expression datasets from TH-MYCN mice

Sympathetic ganglia and tumors from TH-MYCN mice were extracted as described previously (5). Total RNA was extracted using miRNAeasy Mini Kit (Qiagen) and reverse transcribed using Megaplex PreAmp Primers Rodent Pool Set v3.0 (Life Technologies). cDNA was preamplified using human Megaplex PreAmp Primers, Rodent Pool Set v3.0 (Life Technologies) and PreAmp Master mix (Life Technologies).

For mRNA expression, RNA was hybridized to Agilent SurePrint G3 Mouse GE 8 × 60K microarrays. Microarrays and data were summarized and normalized with the vsn method, in the R statistical programming language using the "limma" package (21). Data are available in the ArrayExpress database under accession number E-MTAB-3247.

For miRNA expression, the preamplified samples were loaded into TaqMan Array Rodent MicroRNA A +B Cards Set v3.0 (Life Technologies) and analyzed using the ViiA 7 Real-Time PCR System (Life Technologies). Only C_q values lower than 32 were retained and normalized using global mean normalization, as described previously in ref. 22. Data are available in the ArrayExpress database under accession number E-MTAB-2618.

Expression datasets from human samples/cell lines

Human fetal neuroblasts were isolated from by laser microdissection as described in ref. 23. Samples were obtained with written informed consent from the patients, and studies were conducted in accordance with recognized ethical guidelines (Declaration of Helsinki, Belmont Report). These studies were approved by an institutional review board (Ethics committee Erasme Hospital, Brussels, Belgium; approval no.: OM021). Quantification of 15 candidate miRNAs was done using TaqMan qRT-PCR, data are available in Supplementary Table S2-2. mRNA expression analysis of 649 neuroblastoma tumors was conducted as described previously (24). miRNA expression analysis of 200 neuroblastoma tumors was conducted as described previously (25). For mRNA expression analysis of BE(2)C.miR-204 cells, RNA was isolated 48 hours after treatment with or without doxycycline. RNA was hybridized to Agilent SurePrint G3 Human GE 8 × 60K microarrays. Microarrays and data were summarized and normalized with the vsn method, in the R statistical programming language using the "limma" package (21). Data are available in the NCBI Gene Expression Omnibus database under accession number GSE100658.

Expression analyses

Time-dependent quantification of TH-MYCN expression data was achieved with R software using the "lm" and "MESS" packages. This was either Pi-score as multiple linear model with interaction terms (as described in Fig. 1A), or area under curve. The predicted miRNA–mRNA interaction network was generated using the Bayesian Network with Split-Averaging (BNSA) method, which uses correlated or anti-correlated expression changes in two samples to infer miRNA–mRNA relationships and uses miRNA-target prediction to constrain likely interactions (26). Statistical significance of interactions in the BNSA network is evaluated by resampling using the bootstrapping method (26). Visualization of network was achieved using Cytoscape software. Expression heatmaps were generated with R software, using the "ComplexHeatmap" package. Bar plots were generated with R software using the "ggplot2" package. Kaplan–Meier plots and Cox regression analyses were generated with R software using the "survival" package. Gene set enrichment analyses were conducted with R software using the "fgsea" package (27).

siRNA, miRNA mimic, and stable cell lines

Control siRNA (SI03650318) and siRNAs directed against MYCN (SI03087518 and SI03113670) were purchased from Qiagen. MYCN knockdown was quantified by Western blotting using anti-MYCN antibody sc-53993 (Santa Cruz Biotechnology) at a dilution of 1:2,000. Control miRNA mimic (CN-001000-01) and human miR-204 mimic (C-300563-05) were purchased from Dharmacon. miR-204 expression was quantified using the TaqMan MicroRNA Reverse Transcription Kit and TaqMan MicroRNA Assays (Applied Biosystems). TaqMan assays used in the real-time PCR were #001973 for U6 snRNA endogenous control, #001003 for RNU19 endogenous control, and #000508 for miR-204. Transfection of RNAs was achieved using Lipofectamine 2000 (Invitrogen) according to manufacturer's instructions.

Stable cell lines overexpressing miR-204 were created using human miR-204 lentiviral particles in the SMARTchoice shMIMIC human inducible lentiviral miRNA construct (purchased from Dharmacon, catalog no. VSH6906-224648868). Stable cells were created after lentiviral transduction with 6 μg/mL polybrene and stable selection using puromycin [2 μg/mL or 0.7 μg/mL for BE(2)C and KELLY cells, respectively] for 4 days. Successful lentiviral transductions were confirmed by inducing a passage of each resulting cell lines with doxycycline, and then confirming

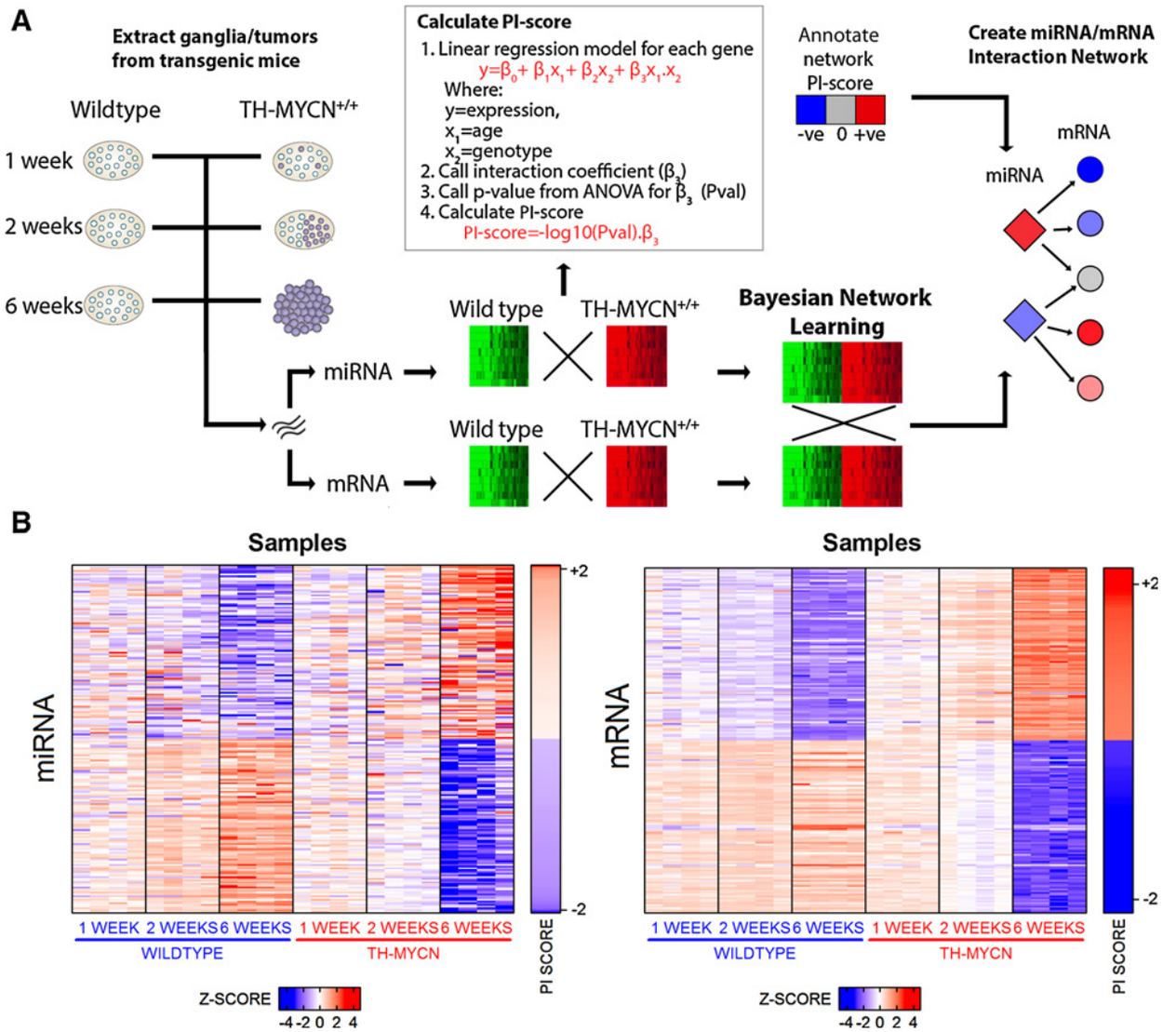

Figure 1.

Gene expression profiling strategy for miRNA and mRNAs in TH-MYCN transgenic mice. **A,** Schematic for the gene expression analyses in this study. Ganglia or tumor were extracted from TH-MYCN$^{+/+}$ mice at time points that correspond to tumor initiation (1 and 2 weeks) or advanced tumors (6 weeks). Gene expression profiling was conducted on miRNA and mRNA derived from these tissues and compared with age-matched control ganglia from wild-type mice (TH-MYCN$^{-/-}$). Quantification of gene expression over time was achieved by calculating the Pi score as described in the figure. miRNA/mRNA networks were resolved using a Bayesian network learning strategy. **B,** Heatmap for expression of miRNA (left) and mRNA (right) in ganglia or tumors derived from wild-type or TH-MYCN$^{+/+}$ mice ($n = 4$ per condition). The top and bottom 100 genes ranked by Pi score are shown for miRNA and mRNA. A positive Pi score means genes are upregulated in TH-MYCN$^{+/+}$ mice, while a negative Pi score means genes are downregulated in TH-MYCN$^{+/+}$ mice. See Supplementary Table S1 for full datasets.

turboGFP expression with fluorescence microscopy and miR-204 overexpression with TaqMan qRT-PCR.

Chromatin immunoprecipitation

Chromatin immunoprecipitation (ChIP) was conducted for MYCN as described previously (13). Briefly, ChIP assays were performed using a ChIP assay kit (Merck Millipore), with a mouse anti-MYCN antibody (Santa Cruz Biotechnology) or a control mouse IgG antibody (Santa Cruz Biotechnology). Real-time PCR analyses of ChIP assay products were performed using primers targeting a negative control region (2362 bp upstream of pre-miR-204 transcription start site), the miR-204 or the *ODC1* gene promoter region. Sequences of primers used in the real-time PCR were 5′ GCCTGGGGAGTATGTGCTTA -3′ (forward) and 5′AGGGTTGGTTCCTCTGGATT -3′ (reverse) for the negative control region; 5′- TGACTCGTGGACTTCCCTTT -3′ (forward) and 5′- GCATTTGATGATGGTGCAAT -3′ (reverse) for the miR-204 promoter region; and 5′- GATGACTTTTGATAGTGAAGTTGAGTTGA -3′ (forward) and 5′- GGCACCGAATTTCACACTGA -3′ (reverse) for the *ODC1* gene promoter region. Fold enrichment

of the miR-204 or ODC1 promoter region by the anti-MYCN antibody was calculated by dividing cycle threshold values of the miR-204 or ODC1 promoter region by cycle threshold values of the negative control region, relative to input.

Biotin-miR-204 pulldown assay

Biotin-labeled miR-204 pulldown assay was adapted from Subramanian and colleagues (28). Briefly, biotin-miR204 or biotin-negative control was transfected into BE(2)C cells for 24 hours and cytoplasmic lysates were taken. At this point, 50-μL samples were removed for input. The remaining lysates derived from these cells were mixed with Dynabeads M-280 Streptavidin (Invitrogen) and washed extensively (28). Input and pulldown RNAs in each sample were eluted and precipitated using a phenol:chloroform:isoamyl alcohol/TRIzol (Invitrogen) protocol (28) and quantified using ND-1000 Spectrophotometer. MYCN and GUSB binding was determined by quantitative PCR comparing abundance in biotin-miR-204 samples compared with biotin-negative control samples. Data presented were normalized to the total mRNA levels for MYCN or GUSB in each respective input sample.

Growth phenotype assays

To measure cell proliferation, the Cell Proliferation ELISA, bromodeoxyuridine (BrdUrd) (colorimetric) Kit (Roche) was used. Colony assays were conducted as described in ref. 13. When using miR-204 mimics, colony assays were seeded 24 hours after transfection. When using miR-204–stable cell lines, doxycycline (1 mg/mL) or DMSO was supplemented into the media and refreshed every 3 days until the end of the experiment.

Animal models

All experimental procedures involving mice were approved by the University of New South Wales Animal Care and Ethics Committee according to the Animal Research Act, 1985 (New South Wales, Australia) and the Australian Code of Practice for Care and Use of Animals for Scientific Purposes (2013). The TH-MYCN transgenic mouse model of neuroblastoma has been described previously (4). Male and female TH-MYCN mice were used in all experiments. For subcutaneous xenograft studies, female BALB/c nude mice (nu/nu) were obtained from the Australian BioResources (Moss Vale, NSW, Australia).

Subcutaneous xenografting and *in vivo* miR-204 imaging

A total of 2×10^6 cells for BE(2)C.miR-204 or 1×10^7 cells for Kelly.miR-204 were subcutaneously injected into the left flank of each BALB/c nude (BALB/c—Fox1nu/Ausb) mice. Mice were monitored and tumor volumes were calculated as $^1/_2 \times \text{length} \times [\text{width}]^2$. When tumor diameter reached 4–5 mm, mice were administered *ad libitum* either 5% sucrose alone (negative control) or 5% sucrose plus 2 mg/mL doxycycline hyclate mice in drinking water. Seven days after the first exposure to supplemented drinking water, tumors were imaged for turboGFP fluorescence using the IVIS SpectrumCT instrument with Living Imaging software on default setting for turboGFP. Mice were euthanized when tumor volume reached 1,000 mm^3 or after 12 weeks had passed since injection. Tumors were extracted and miR-204 expression was quantified using TaqMan qRT-PCR as described previously.

Data and materials availability

Gene expression omnibus accessions: # GSE45547, GSE71060, and GSE71061. ArrayExpress accessions E-MTAB-3247 and E-MTAB-2618.

Statistical analysis

Unless otherwise stated, all statistical analysis was conducted in GraphPad Prism 6 software, and *P* values were determined using unpaired two-sided *t* tests. *P* values less than 0.05 were considered significant [ns, not significant ($P > 0.05$), *, $P < 0.05$; **, $P < 0.01$; ***, $P < 0.001$].

Results

Gene expression profiling of miRNA and mRNA in TH-MYCN transgenic mice

To evaluate miRNA/mRNA expression in neuroblastoma, we conducted transcriptomic analyses of ganglion tissues derived from the TH-MYCN transgenic mice. We isolated premalignant sympathetic ganglia or tumors from TH-$MYCN^{+/+}$ mice at 1, 2, and 6 weeks of age, as well as age-matched ganglia from normal littermate wild-type mice (Fig. 1A). We conducted gene expression profiling on these samples for both miRNA and mRNA expression patterns (29). To quantify time-dependent changes in expression of miRNA or mRNAs, we assigned a "Pi-score" (29). The Pi-score was determined by fitting a multiple linear model to each miRNA or mRNA expression value and determining the interaction coefficient of the two independent variables within the dataset, that is, age (1, 2, or 6 weeks) and genotype (TH-$MYCN^{+/+}$ or wild-type; Fig. 1A). All expression data for miRNAs and mRNAs were then evaluated by heatmap plotting to validate that the Pi-score ranked gene expression changes are correlated with relative expression change over time (Fig. 1B; Supplementary Table S1). We also evaluated another method of time-dependent quantitation, by determining the net difference between TH-MYCN and wild-type area under curve (ΔAUC). Pi scores and ΔAUC values demonstrated similar expression trends, and were strongly correlated (Supplementary Fig. S1A and S1B). However, Pi scores were more effective at quantifying linear growth trends than ΔAUC (Supplementary Fig. S1C and S1D).

Identification of miRNA–mRNA interaction networks

Next, we conducted integrative analysis of expression data to identify miRNA–mRNA interaction networks (Fig. 1A; Fig. 2A). We used a Bayesian network learning model that takes into account the statistical significance of correlated expression patterns between miRNA and mRNA pairs, as well as prediction of miRNA seed sequence mediating binding to mRNA targets (using the TargetScanMouse database; ref. 26). For this network analysis, we used selection criteria as follows: (i) to bias toward miRNA–mRNA interactions that are inhibitory in nature, only negatively correlated interactions were included, and (ii) to identify interactions most crucial to early stages of tumorigenesis, we used only data from weeks 1 and 2, which in TH-$MYCN^{+/+}$ mice corresponds to the premalignant phase of tumor development (1, 5, 9). In addition, Pi score was used to quantify whether expression of miRNA–mRNAs was up- or downregulated through tumorigenesis.

Network analysis identified 19 significant miRNA–mRNA interaction subnetworks (Fig. 2A; Supplementary Table S2-1). The network consisted of four major hubs: (i) a miR-18a hub, (ii)

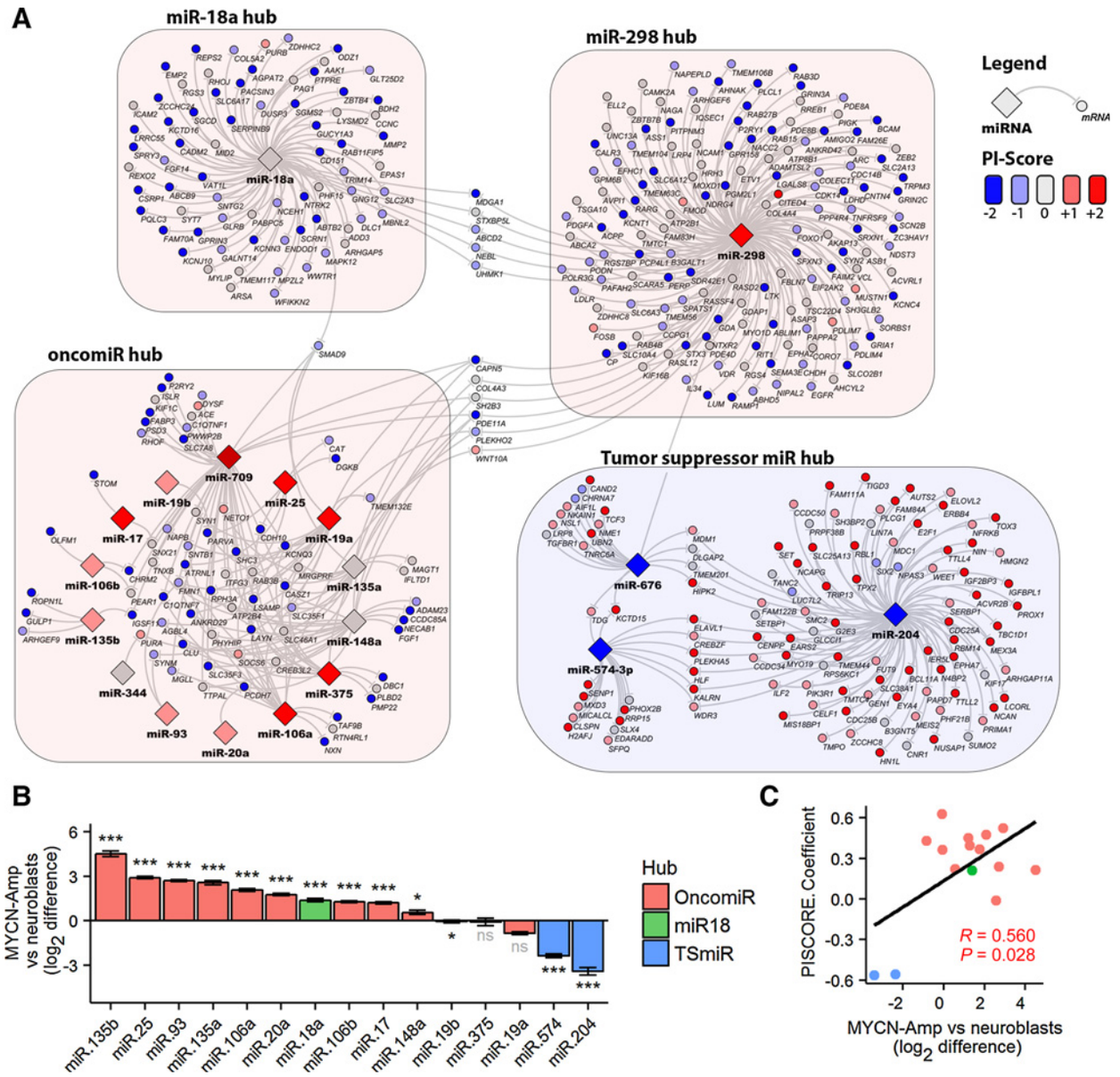

Figure 2.

mRNA–miRNA interaction network from TH-MYCN$^{+/+}$ mice. **A,** Network was resolved using a Bayesian network learning strategy and visualized using Cytoscape software. miRNA (diamonds) and their predicted target mRNAs (circles) are shown by connecting lines. The color of each miRNA and mRNA is annotated by Pi score. Hubs were devised on the basis of miRNAs that shared multiple common mRNA targets. See Supplementary Table S2-1 for specific miRNA–mRNA interactions. **B,** Difference in miRNA $\log_2$ expression values for *MYCN*-amplified tumors ($n = 20$) compared with the average expression in human fetal neuroblast samples ($n = 7$). *P* value was calculated using two-sided *t* test comparing miRNA expression between *MYCN*-amplified tumors and human fetal neuroblasts. ns, not significant; $P > 0.05$; *, $P < 0.05$; **, $P < 0.01$; ***, $P < 0.001$. **C,** Correlation charts for Pi score interaction coefficient and $\log_2$ difference between *MYCN*-amplified tumors and human fetal neuroblasts (as in **B**). *P* value and R value calculated by Pearson correlation tests.

a miR-298 hub, (iii) an "oncomiR" hub and (iv) a "Tumor suppressor miR" hub (Fig. 2A). On the basis of Pi-score, the miRNA's in the first three hubs demonstrated expression patterns that fit with a tumor promotion function, while the miRNA's in the Tumor suppressor miR hub (mir-204/miR-676/mir-574-3p) demonstrated expression patterns that fit with a tumor-repressive function (Fig. 2A; Supplementary Fig. S2).

To validate that miRNAs in the interaction networks derived from TH-MYCN mouse tissues showed similar expression characteristics in human samples at tumor initiation, we compared their expression patterns in human fetal neuroblasts and MYCN-amplified neuroblastomas, thus contrasting the cell-of-origin tissues with end-stage malignancy. We used miRNAs that have a human homolog that demonstrated conservation of the 6-mer

seed sequence when compared with the mouse miRNA. This reduced our candidate miRNAs from 19 in the TH-MYCN tumorigenesis network to 15 miRNAs in human samples. Examination of the expression of these 15 miRNAs in human fetal neuroblasts demonstrated that the expression characteristics were similar between human and mouse samples, with the majority of miRNA members from the oncomiR hub showing upregulation in human *MYCN*–amplified neuroblastoma compared with human fetal neuroblasts, whereas the tumor suppressor miR (TSmiR) hub members showed marked downregulation in *MYCN*-amplified tumors compared with fetal neuroblasts, in particular miR-204 (Fig. 2B; Supplementary Table S2-2). Moreover, the coefficient used to derive the Pi score in the murine analysis showed a significant correlation with the extent of miRNA upregulation in human *MYCN*-amplified tumors compared with human neuroblasts (Fig. 2C). These data therefore show that expression patterns of miRNAs identified in our network analysis at tumor initiation from TH-MYCN mouse ganglia were recapitulated in analogous human tissues.

Evaluation of miRNA and miRNA target gene signatures in human neuroblastoma tumors

We then evaluated the expression of our predicted TH-MYCN interaction networks in two human neuroblastoma tumor cohorts (24, 25). For this, we analyzed the expression of miRNAs, as well as their predicted target mRNAs (hereafter referred to as miRNA target signatures; Fig. 3A). Hierarchical clustering of gene expression data showed that in both miRNA and miRNA target signatures, tumor suppressor hub members miR-204 and miR-574 diverged considerably from members of the other hubs (Fig. 3A). When considering the expression of both the individual miRNA and its predicted target signature, expression patterns suggested that tumor suppressor hub miRNAs were negatively associated with *MYCN*-amplification while the majority of oncomiR members were positively associated with *MYCN* amplification (Fig. 3B). Similarly, Cox regression analysis for miRNAs, their target gene signatures, and patient survival suggested that high expression of tumor suppressor hub miRNAs was associated with good patient outcome, while high expression of most oncomiR members was associated with poor patient outcome (Fig. 3C; Supplementary Fig. S3A–S3C). To quantify the magnitude of association with *MYCN* amplification or patient survival for each miRNA used in the above comparisons, the difference between the miRNA and miRNA target signatures was evaluated [i.e., difference = (miRNA value)−(miRNA signature value)]. The miRNA with the greatest absolute difference in both analyses was miR-204 (Fig. 3D and E; Supplementary Fig. S3D, see arrow). miR-204 was therefore chosen for more extensive mechanistic and functional analyses.

MYCN binds the miR-204 promoter and represses its transcription

As miR-204 was strongly repressed in TH-MYCN$^{+/+}$ compared with wild-type samples (Supplementary Table S1), we hypothesized that miR-204 may be a MYCN transcriptional target gene. Consistent with this prediction, miR-204 expression was shown to be increased in MYCN siRNA-treated neuroblastoma cell lines (Fig. 4A). Moreover, gene-set enrichment analysis (GSEA) showed that target genes of miR-204 (predicted in the TH-MYCN network) were downregulated upon MYCN siRNA treatment of neuroblastoma cells, suggesting that MYCN had a negative influence on miR-204 activity (Supplementary Fig. S4). To evaluate whether MYCN is a direct regulator of miR-204, we conducted chromatin immunoprecipitation PCR on a MYCN-amplified human neuroblastoma cell line, BE(2)-C. We found that MYCN protein binding was enriched at the gene promoter of miR-204 to a similar magnitude as the well-known MYCN transactivation target gene, ornithine decarboxylase-1 (ODC1; Fig. 4B and C; ref. 30). MYCN binding occurred in the vicinity of a canonical Ebox binding motif (CATGTG - 17 bp downstream from the pre-miR-204 transcriptional start site) and a noncanonical Ebox binding motif (CATTTG – 137 bp downstream from the pre-miR-204 transcriptional start site), suggesting possible Ebox-mediated binding for MYCN transcriptional repression of miR-204.

miR-204 directly binds MYCN mRNA and inhibits its expression

Next we evaluated the consequence of miR-204 overexpression in human neuroblastoma cell lines. We created two doxycycline-inducible miR-204–overexpressing cell lines from MYCN-amplified neuroblastoma cell lines, BE(2)C and KELLY (henceforth named BE(2)C.miR-204 and KELLY.miR-204 cells, respectively; Supplementary Fig. S5A and S5B). GSEA on gene expression microarrays for doxycycline treated versus doxycycline-untreated BE(2)C.miR-204 cells identified that a number of MYC-related gene sets were all significantly downregulated with miR-204 overexpression (Fig. 5A). Furthermore, GSEA of our own curated BE(2)C MYCN target signatures, showed that miR-204 overexpression was associated with reduced MYCN activity (i.e., the expression of positively regulated MYCN targets was repressed, while the expression of negatively regulated MYCN targets was increased; Fig. 5B). This finding was confirmed by GSEA using MYCN-positive target genes identified by ChIP-sequencing (Supplementary Fig. S5C; ref. 31). This finding suggests that miR-204 could be a negative regulator of MYCN signaling. Indeed, we found that miR-204 overexpression, demonstrated a significant downregulation of MYCN protein expression upon doxycycline inducible miR-204 overexpression in BE(2)C.miR-204 and KELLY.miR204 cells (Fig. 5C; Supplementary Fig. S5D). Based upon the RNA22 miRNA binding database, miR-204 was predicted to bind the coding region of the MYCN mRNA transcript (Supplementary Fig. S5E). To confirm direct binding of miR-204 to MYCN we used a streptavidin-biotin pulldown strategy to investigate whether miR-204 physically bound to MYCN mRNA (Fig. 5D). This demonstrated that MYCN was enriched by the biotin-miR-204 bait construct, while on the other hand, negative control GUSB was not enriched (Fig. 5D). Together these data suggest that miR-204 directly binds the coding region of MYCN mRNA, causing its degradation, and a consequent reduction of MYCN expression in neuroblastoma cells.

miR-204 overexpression represses neuroblastoma cell proliferation and tumor development

To evaluate the function of miR-204 in neuroblastoma, we next evaluated the phenotypic effect of miR-204 overexpression on human neuroblastoma cell lines with differing levels of MYCN. We used a panel of *MYCN*-amplified and *MYCN* nonamplified cell lines, as well as SHEP21N cells, which allow for doxycycline-inducible knockdown of MYCN (Supplementary Fig. S6A). Transfection of miR-204 mimics into *MYCN*-amplified BE(2)C, KELLY and IMR32 neuroblastoma cells was accompanied by a significant

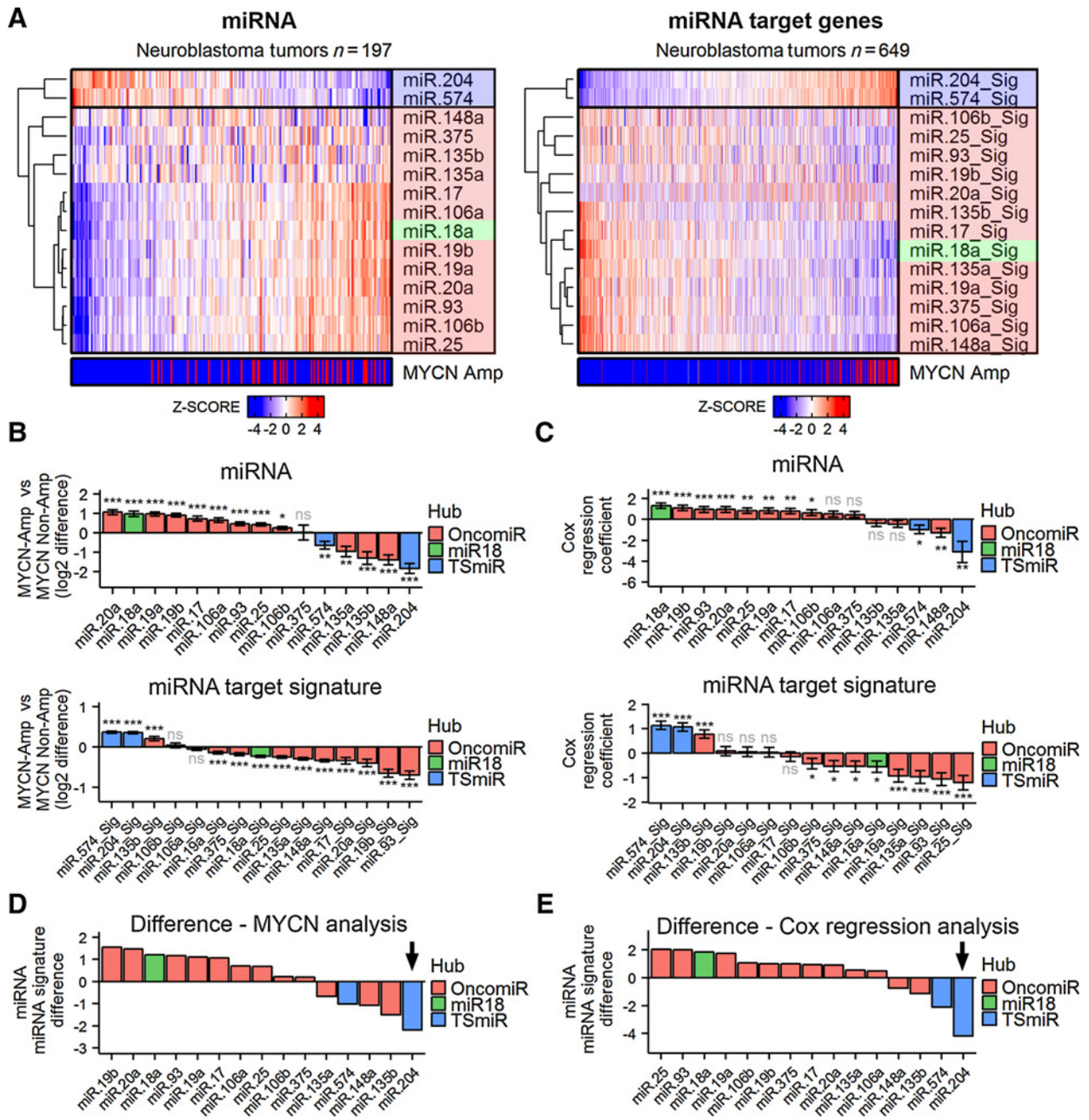

Figure 3.

Analysis of miRNA and miRNA target signatures in human neuroblastoma. **A,** Heatmap of miRNA (left) and miRNA target signatures (right) in human neuroblastoma samples (24, 25). Target signatures for each miRNA were created on the basis of the expression of predicted target genes identified in Fig. 2. Expression of each signature was calculated on the basis of the mean-scaled $\log_2$-adjusted expression value of all mRNAs in the signature. *MYCN*-amplified tumors are annotated in red and *MYCN* nonamplified tumors in blue at the bottom ("MYCN Amp"). miRNA and miRNA target signatures are arranged in rows by hierarchical clustering. **B,** The $\log_2$ difference in expression for miRNA (top) or miRNA target signatures (bottom) was determined in *MYCN*-amplified tumors versus *MYCN* nonamplified tumors. *P* value was calculated using two-sided test comparing expression between *MYCN*-amplified tumors and *MYCN* nonamplified tumors. ns, not significant; $P > 0.05$; *, $P < 0.05$; **, $P < 0.01$; ***, $P < 0.001$. **C,** Univariate Cox regression analysis was conducted for miRNA (top) and miRNA target signatures (bottom) in relation to predicting overall survival of patients with neuroblastoma. Displayed is the Cox regression coefficient for patients based on high versus low expression of miRNAs or miRNA target signatures. High expression was determined as the top quartile of tumors ranked by expression, whereas the low expression group was determined as the bottom three quartiles of tumors ranked by expression. *P* value determined for Cox regression coefficient for effect of miRNA or miRNA target signature for patient outcome. ns, not significant; $P > 0.05$; *, $P < 0.05$; **, $P < 0.01$; ***, $P < 0.001$. **D,** miRNAs were ranked by the difference between miRNA and miRNA target signatures determined in the *MYCN* amplification analysis in **B**. Arrow, miR-204 has the greatest absolute difference. **E,** miRNAs were ranked by the difference between miRNA and miRNA target signatures determined in Cox regression analysis in **C**. Arrow, miR-204 has the greatest absolute difference.

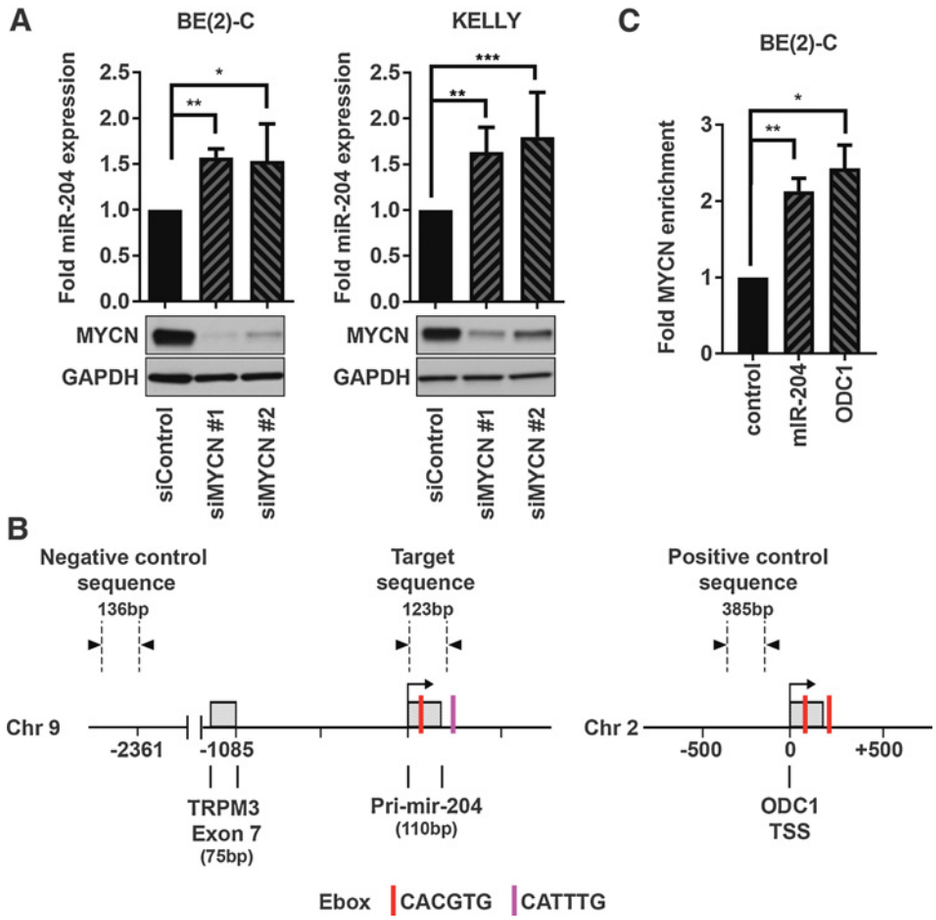

Figure 4.

MYCN represses miR-204 expression. **A,** miR-204 expression with MYCN knockdown. siRNA's directed against MYCN were transfected into BE(2)C and KELLY neuroblastoma cells and 24 hours after transfection, miR-204 expression was measured by real-time PCR. MYCN knockdown was confirmed by Western blotting compared with nontargeting siRNAs. GAPDH was used as a loading control. Data displayed reflect the mean relative expression of miR-204 compared with control siRNA-treated samples from three biological replicates. *, $P < 0.05$; **, $P < 0.01$; ***. $P < 0.001$. P value was calculated using two-sided t test. **B,** Schematic of ChIP-PCR strategy for MYCN enrichment. TSS, transcription start site. **C,** ChIP-PCR in BE(2)C cells for MYCN binding at the miR-204 promoter. Relative MYCN enrichment was calculated for miR-204 and ODC1 promoter by dividing PCR products from target primers by PCR products from primers targeting the negative control region. Data displayed represent the average MYCN enrichment at target regions ± SE from three biological replicates. *, $P < 0.05$; **, $P < 0.01$.

decrease in cell proliferation, as measured by BrdUrd incorporation (Fig. 6A; Supplementary Fig. S6B). However, a similar experiment in 4 *MYCN* nonamplified cell lines, SHEP, SK-N-AS, SH-SY5Y and SK-N-FI, showed no inhibition of BrdUrd incorporation, suggesting miR-204 inhibition of proliferation is selective for cells with high levels of MYCN (Fig. 6A; Supplementary Fig. S6B). Indeed, using SHEP21N cells, which allow for doxycycline-inducible knockdown of stably incorporated MYCN, showed that miR-204 is more inhibitory in the MYCN-high expressing condition compared with the MYCN-low expressing condition (Fig. 6B; Supplementary Fig. S6C). Similarly, miR-204 mimics and doxycycline-inducible overexpression of miR-204 significantly decreased the colony-forming capacity of MYCN-amplified BE(2)C and KELLY cells (Fig. 6C; Supplementary Fig. S6D), whereas in *MYCN* nonamplified cells SHEP and SK-N-FI, colony number was not significantly decreased with overexpression of miR-204 mimics (Supplementary Fig. S6D). Importantly, these findings regarding miR-204 selectivity against MYCN-expressing cells were replicated *in vivo,* where subcutaneous tumor xenografts of BE(2)C.miR-204 and KELLY.miR-204 induced to overexpress miR-204 by exogenously administered doxycycline showed significant delays in tumorigenesis compared with tumors arising in control mice that did not receive doxycycline (Fig. 6D; Supplementary Fig. S6E–S6G). These findings demonstrate that miR-204 selectively inhibits *MYCN*-amplified neuroblastoma cell proliferation *in vitro* and *in vivo*.

Discussion

Unravelling the mechanism by which MYCN promotes tumorigenesis remains a significant biological challenge to neuroblastoma research, and highlights the need for mechanistic studies so that ultimately therapeutic vulnerabilities of MYCN can be targeted. Here, using an integrative gene expression analysis approach, we have identified miRNA–mRNA expression subnetworks that are active during neuroblastoma tumorigenesis. We were able to validate these miRNA–mRNA subnetworks for their relevance to human neuroblastoma by establishing their strong association with *MYCN* amplification and patient prognosis. From this analysis, we then confirmed that a candidate tumor suppressor, miR-204, indeed directly binds MYCN mRNA, repressing MYCN expression in neuroblastoma cells, thus causing inhibition of neuroblastoma cell growth *in vitro* and tumorigenesis *in vivo*.

We used a Bayesian learning model to derive a miRNA–mRNA interaction network. This model has significant advantages to identify potential interaction partners by considering the correlation of expression values for miRNA–mRNA pairs across wild-type and TH-MYCN$^{+/+}$ samples and also the predicted complementarity of the miRNA seed sequence (26). We then annotated each member of the network according to Pi-score. The advantage of the Pi-score method compared with pairwise differential expression is that is summarizes gene expression changes for both

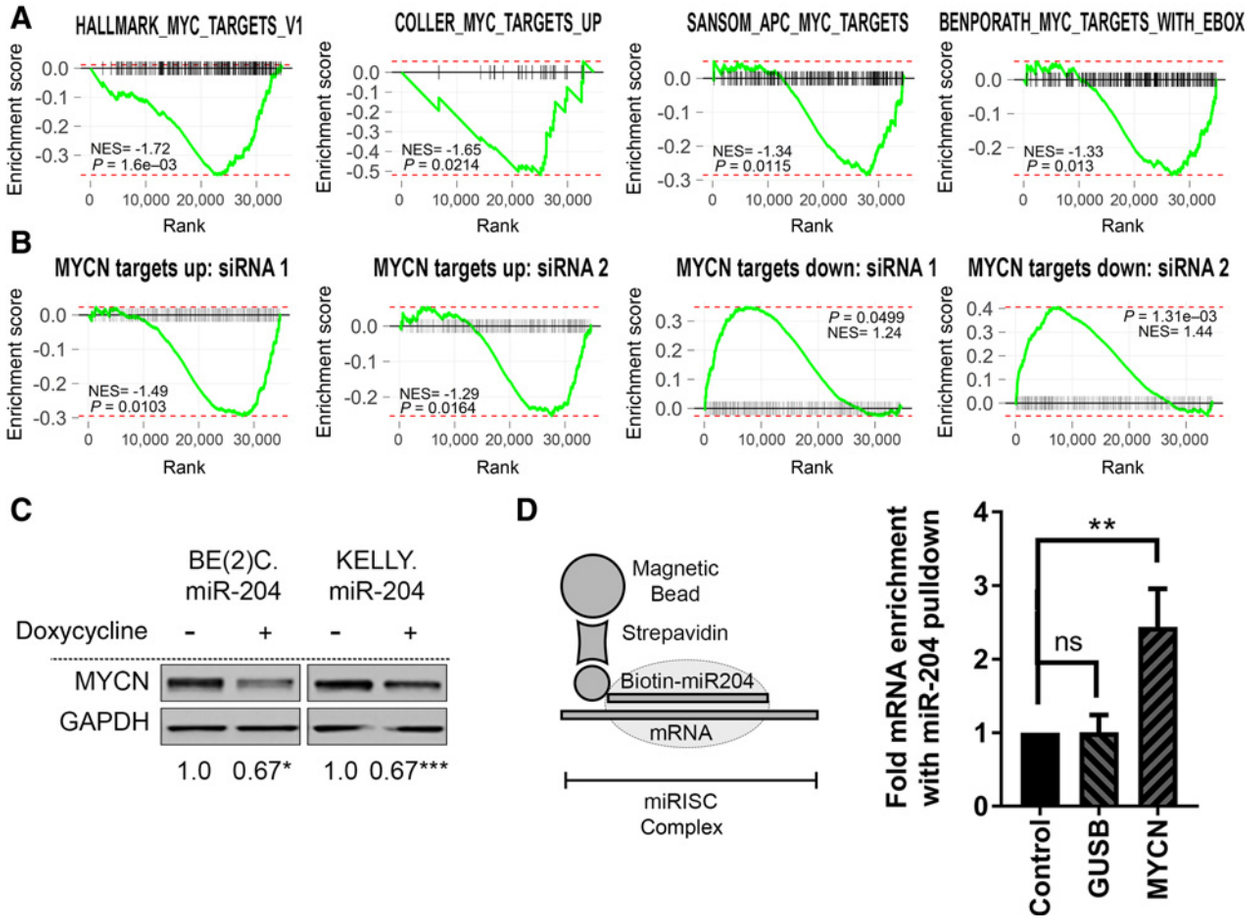

Figure 5.

MYCN is a miR-204 target gene. **A,** MYC-related GSEA plots based on the ranked gene expression data from doxycycline-treated versus doxycycline-untreated BE(2)C.miR-204 cells. Selected MYC-related gene sets are displayed. Gene sets are available in the Molecular Signatures Database. NES, normalized enrichment score. **B,** MYCN-related GSEA plots based on the ranked gene expression data from BE(2)C.miR-204 cells in **A**. Gene sets for MYCN target genes were curated from BE(2)C cells treated with MYCN siRNAs. Data is available at GEO accession numbers GSE71060 and GSE71061. Target genes that are upregulated by MYCN ("MYCN targets up") or downregulated by MYCN ("MYCN targets down") were considered the 500 most down- or upregulated genes upon MYCN siRNAs, respectively. **C,** Western blots for MYCN expression in BE(2)C.miR-204 or KELLY.miR-204 with miR-204 overexpression. miR-204 expression was achieved by treating cells with doxycycline. MYCN expression was quantified using densitometry relative to each cell line's respective treatment control and normalized according to GAPDH loading control. Densitometry was determined across three biological replicates for each cell line. *, $P < 0.05$; **, $P < 0.01$; ***, $P < 0.001$. P value was calculated using two-sided t test on densitometry results (see Supplementary Fig. S5D). **D,** Biotin-conjugated miR-204 was immobilized on streptavidin beads and miR-204–bound mRNAs were enriched from the lysates of BE(2)C cells. Left, schematic of the biotin-tagged miRNA pulldown of target mRNA as part of the miRNA-associated RNA-induced silencing complex (miRISC). Right, real-time PCR results for miRNA pulldowns using miR-204 as bait. Specific primers designed for MYCN or GUSB (negative control) were used to calculate their relative enrichment in miR-204 pulldowns compared with control. Data displayed was determined from the average of three biological replicates ± SE. **, $P < 0.01$, ns, not significant ($P > 0.05$), calculated by two-sided t test.

genotypes over time as a single metric and it quantifies time-dependent gene expression changes by evaluating their linear trend. Using this method, we could confirm miRNA–mRNA interactions in the network, which had contrary expression changes to identify miRNA–mRNA interactions that were more likely to be inhibitory.

To prioritize miRNAs for biological investigation, we analyzed miRNAs and their predicted mRNA targets in human tumor samples. Two important clinical characteristics were used to quantify the influence of miRNAs and miRNA signatures: (i) differential expression in *MYCN*-amplified patients and (ii) differential time of survival (as measured by Cox regression coefficients). To prioritize miRNA for further biological validation, we used the greatest absolute difference of miRNAs compared with their target mRNAs in these analyses. This metric was selected to shortlist interactions that conform to the canonical miRNA mechanism of action, that is, inhibiting its mRNA targets. From this analysis, miR-204 was selected for having the greatest absolute difference between the miRNA and miRNA signature in both types of analysis, thus supporting our rationale to explore in further biological assays. It is important to note though, while our subsequent biological analyses of miR-204 validated this approach, it is distinctly possible that other miRNAs have equally important functions in regulation of tumorigenesis as small

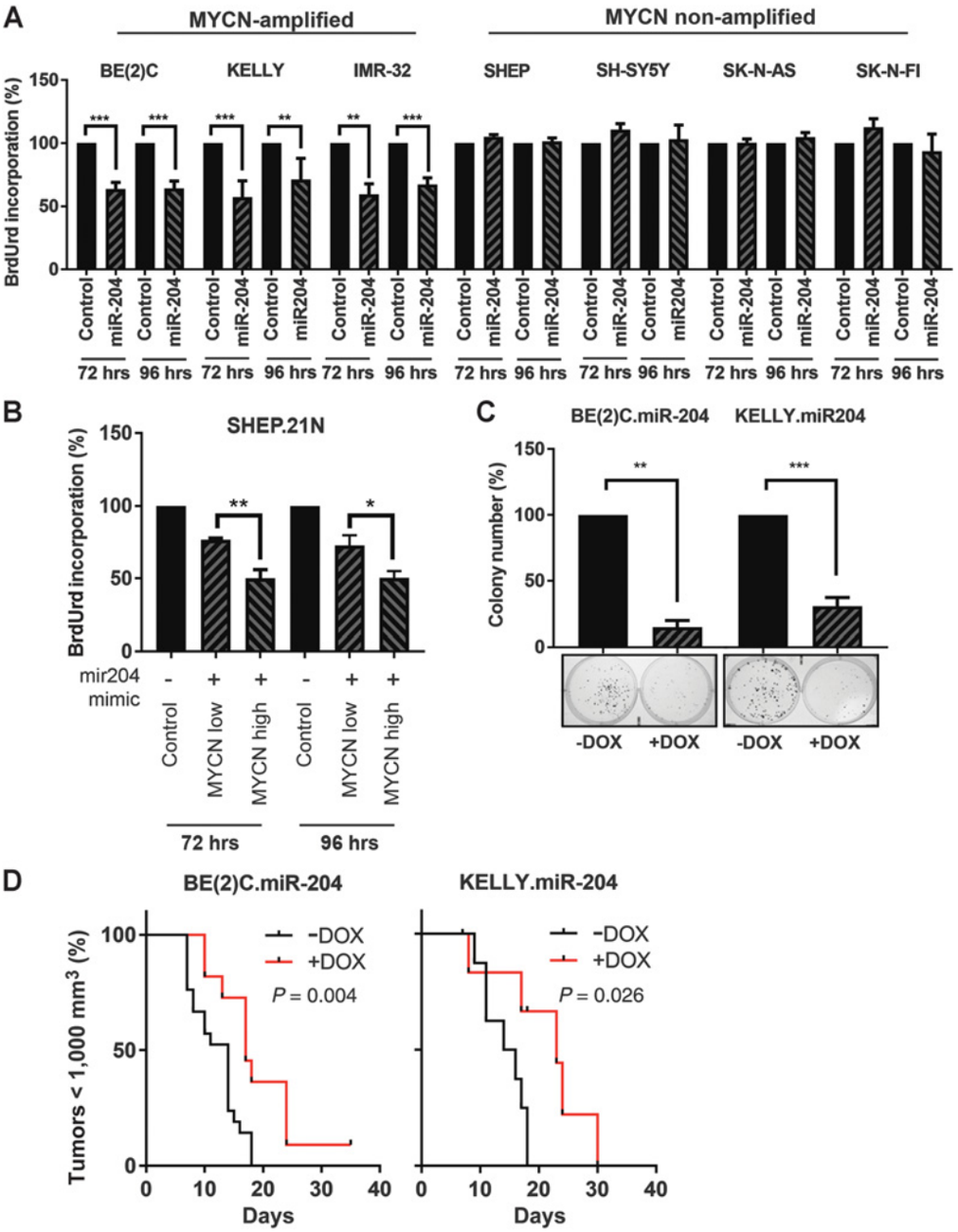

Figure 6.

miR-204 inhibits neuroblastoma cell proliferation and tumor growth. **A,** BrdUrd incorporation assays in *MYCN*-amplified and *MYCN* nonamplified cells transfected with a miR-204 mimic. All data from miR-204 mimic are normalized relative to control mimic. Data displayed was determined from the average of three biological replicates ± SE. **, $P < 0.01$; ***, $P < 0.001$, calculated by two-sided *t* test. **B,** BrdUrd incorporation assays in SHEP21N cells. All data from miR-204 mimic is normalized relative to control mimic. MYCN-low condition refers to cells treated with 1 mg/mL doxycycline in growth media, while MYCN-high condition refers to DMSO in growth media. Data displayed were determined from the average of three biological replicates ± SE. *, $P < 0.05$; **, $P < 0.01$, calculated by two-sided *t* test. **C,** Colony-forming assays in BE(2)C.miR-204 and KELLY.miR-204 cells. In BE(2)C.miR204 or KELLY.miR204 cells, miR-204 overexpression was achieved by treating cells with doxycycline (DOX), which was refreshed in fresh media every three days until the end of the assay. Colony number percentage was determined compared with the control condition, from the average of three biological replicates ± SE. Representative images for colony number are displayed at the bottom. **, $P < 0.01$; ***. $P < 0.001$, calculated by two-sided *t* test. **D,** Kaplan–Meier plots from xenograft tumor growth assays for BE(2)C.miR204 and KELLY.miR204 cells with or without miR-204 overexpression. Xenograft tumors were established in BALB/c nu/nu mice and miR-204 expression was induced in each cell line by supplementing drinking water with doxycycline and sucrose (+DOX) compared with control mice, who were fed sucrose-supplemented water (−DOX). Water was administered *ad libitum*. miR-204 overexpression was determined by green fluorescent protein fluorescence in +DOX-treated mice compared with −DOX-treated mice (see Supplementary Fig. S6A and S6B). Time until maximum tumor burden (1,000 mm^3) was then determined for all mice. Differences in time until maximum tumor burden due to miR-204 overexpression was calculated using log-rank tests, with *P* values as indicated.

miRNA expression changes may have profound impact due to coordinated changes in multiple target gene levels. Indeed, within the interaction network, there were a number of predicted interactions, for which there is already strong evidence in the literature. For instance, the miR-17–92 cluster members and its paralogs from the miR-106a-363 and miR-106b-25 clusters accounted for 8 of 14 miRNA members of the "oncomiR hub," consistent with their established role as oncogenic miRNAs (32). Moreover, many of these miRNAs are known to be positively regulated by MYC(N) transcriptional activity, and have been identified to promote neuroblastoma pathogenesis (33). Our analysis of miRNA expression and miRNA target signatures for oncomiRs in human tumors mostly confirmed what is known about the miRNAs in neuroblastoma, with a general positive association between the oncomiRs and *MYCN* amplification. These findings are useful as they support the validity of our network methodology. In addition, the possibility remains that while miR-204 was the focus of our investigation, other members of the "tumor suppressor hub," could have synergistic effects on cell functions by virtue of their common predicted mRNA targets. Further research to deconvolute the contributions of network members will be a valuable future study to appreciate the biological relevance of these findings from a systems-level perspective.

On the basis of our human tumor analysis of miRNA and miRNA target signatures, we then confirmed that miR-204 has a tumor suppressor role in neuroblastoma. In agreement, most functional studies that have explored miR-204 function in cancer cells have demonstrated that miR-204 overexpression inhibits cancer viability, proliferation, drug resistance, or migration/invasion (34–37). However, this tumor-suppressive role appears to be somewhat context-dependent and in rarer cases such as in prostate cancer, miR-204 has a dual role and can act as an oncogene in some cell lines (38, 39). This context dependence is likely explained by variable expression patterns of target genes in particular cell types. In our study, we showed that MYCN is a direct target gene of miR-204 and this may govern why miR-204 functions as a tumor suppressor in neuroblastoma cell lines. The novel interaction between miR-204 and MYCN has potential implications for other cancers that present with *MYCN* amplification or overexpression, such as medulloblastoma or neuroendocrine prostate cancer (40, 41). Moreover, it will be important to explore whether miR-204 also regulates the highly conserved MYCN homolog, MYC, which is deregulated in approximately half of all human cancer.

We identified miR-204 as a transrepression target of MYCN, where ChIP assays demonstrated that MYCN directly bound near Ebox-binding motifs in the pre-miR-204 gene promoter of chromosome 9. MYCN can drive transrepression through multiple mechanisms. Direct DNA binding of MYCN to Ebox-binding motifs can lead to recruitment of histone methylation complex PRC2 to prepress chromatin accessibility (42). In addition, MYCN can tether to DNA indirectly by physically binding other DNA binding transcription factors such as MIZ1 and SP1, which can lead to histone deacetylase recruitment and chromatin silencing (43–45). Notably these mechanisms of MYC(N)-driven transrepression represent promising anticancer targets and are the focus of numerous preclinical studies (42, 46–48). Future work will unveil mechanisms by which MYCN represses miR-204 expression so that miR-204 reactivation therapies can be conceived for MYCN-driven neuroblastoma.

We also showed that miR-204 physically bound and repressed MYCN mRNA. RNA22 predicted binding to the MYCN coding region, thus explaining why recent MYCN 3′ UTR binding screens failed to detect miR-204 binding to MYCN (29). As miR-204 is downregulated by MYCN in neuroblastoma cells, this permits MYCN to maintain its expression at a continued high level through tumor initiation and progression. Our findings therefore suggest that for *MYCN* amplification to achieve its "driver" potential in tumorigenesis, part of its mechanism is to inhibit miR-204 expression, thereby reinforcing its own expression levels by preventing miR-204–mediated negative feedback. This finding reflects much of the literature, which has identified multiple independent mechanisms by which MYCN expression is maintained at high levels in neuroblastoma cells, whether it is by mechanisms that drive *MYCN* gene transcription, mRNA stability/translation, or protein stability (8, 13, 49–52). As *MYCN* amplification already generates very high MYCN expression, these findings collectively suggest MYCN-driven tumorigenesis is dependent on excessive MYCN levels in the face of many normal cellular mechanisms that aim to reduce MYCN levels. These observations highlight a potential susceptibility of neuroblastoma cells for therapeutic measures that restore endogenous MYCN inhibitors such as miR-204 or inhibit mechanisms that promote high MYCN levels (13, 49, 50, 53, 54). Whether miR-204 could be used as a novel therapeutic strategy to target MYCN expression remains to be determined. Future work should address potential therapeutic strategies to reactivate miR-204 expression in neuroblastoma or gene therapy alternatives in which miR-204 could be delivered as an exogenous therapeutic.

In this study, we have used a miRNA–mRNA interaction network approach to identify miR-204 as a candidate tumor suppressor in neuroblastoma. We describe a novel double negative feedback loop between MYCN and miR-204 in neuroblastoma cells and identify miR-204 as an inhibitor of neuroblastoma proliferation *in vitro* and *in vivo*.

Disclosure of Potential Conflicts of Interest

No potential conflicts of interest were disclosed.

Authors' Contributions

Conception and design: C.Y. Ooi, D.R. Carter, A. Beckers, B.B. Cheung, G.M. Marshall

Development of methodology: C.Y. Ooi, D.R. Carter, B. Liu, A. Beckers, A. Lalwani, Z. Nagy, S.D. Brouwer, T. Liu, B.B. Cheung, G.M. Marshall

Acquisition of data (provided animals, acquired and managed patients, provided facilities, etc.): C.Y. Ooi, D.R. Carter, A. Beckers, Z. Nagy, K.D. Preter, F. Speleman, G.M. Marshall

Analysis and interpretation of data (e.g., statistical analysis, biostatistics, computational analysis): C.Y. Ooi, D.R. Carter, B. Liu, C. Mayoh, A. Beckers, A. Lalwani, Z. Nagy, T. Liu, K.D. Preter, F. Speleman, B.B. Cheung, G.M. Marshall

Writing, review, and/or revision of the manuscript: C.Y. Ooi, D.R. Carter, C. Mayoh, A. Beckers, M.D. Norris, M. Haber, K.D. Preter, F. Speleman, B.B. Cheung, G.M. Marshall

Administrative, technical, or material support (i.e., reporting or organizing data, constructing databases): C.Y. Ooi, D.R. Carter, B. Decaesteker, T.-T. Hung

Study supervision: C.Y. Ooi, D.R. Carter, B.B. Cheung

Acknowledgments

The authors acknowledge the facilities, and the scientific and technical assistance of the National Imaging Facility at the UNSW node. M.D Norris, M. Haber, and G.M. Marshall received: NHMRC Australia (Program grant, grant #APP1016699); Cancer Institute NSW (program grants #10/TPG/1-03 #14/TPG/1–13). D.R. Carter received Cancer Institute NSW (Early Career

Fellowship - #DC000594). C-Y. Ooi received Australian Postgraduate Award and Josee Hilton PhD excellence award.

The costs of publication of this article were defrayed in part by the payment of page charges. This article must therefore be hereby marked *advertisement* in accordance with 18 U.S.C. Section 1734 solely to indicate this fact.

Received October 8, 2017; revised February 7, 2018; accepted March 28, 2018; published first April 2, 2018.

References

1. Marshall GM, Carter DR, Cheung BB, Liu T, Mateos MK, Meyerowitz JG, et al. The prenatal origins of cancer. Nat Rev Cancer 2014;14:277–89.
2. Matthay KK, Maris JM, Schleiermacher G, Nakagawara A, Mackall CL, Diller L, et al. Neuroblastoma. Nat Rev Dis Primers 2016;2:16078.
3. Chesler L, Weiss WA. Genetically engineered murine models–contribution to our understanding of the genetics, molecular pathology and therapeutic targeting of neuroblastoma. Semin Cancer Biol 2011;21:245–55.
4. Weiss WA, Aldape K, Mohapatra G, Feuerstein BG, Bishop JM. Targeted expression of MYCN causes neuroblastoma in transgenic mice. EMBO J 1997;16:2985–95.
5. Hansford LM, Thomas WD, Keating JM, Burkhart CA, Peaston AE, Norris MD, et al. Mechanisms of embryonal tumor initiation: distinct roles for MycN expression and MYCN amplification. Proc Natl Acad Sci U S A 2004; 101:12664–9.
6. Alam G, Cui H, Shi H, Yang L, Ding J, Mao L, et al. MYCN promotes the expansion of Phox2B-positive neuronal progenitors to drive neuroblastoma development. Am J Pathol 2009;175:856–66.
7. Beckers A, Van Peer G, Carter DR, Gartlgruber M, Herrmann C, Agarwal S, et al. MYCN-driven regulatory mechanisms controlling LIN28B in neuroblastoma. Cancer Lett 2015;366:123–32.
8. Molenaar JJ, Domingo-Fernandez R, Ebus ME, Lindner S, Koster J, Drabek K, et al. LIN28B induces neuroblastoma and enhances MYCN levels via let-7 suppression. Nat Genet 2012;44:1199–206.
9. Calao M, Sekyere EO, Cui HJ, Cheung BB, Thomas WD, Keating J, et al. Direct effects of Bmi1 on p53 protein stability inactivates oncoprotein stress responses in embryonal cancer precursor cells at tumor initiation. Oncogene 2012;32:3616–26.
10. Teitz T, Inoue M, Valentine MB, Zhu K, Rehg JE, Zhao W, et al. Th-MYCN mice with caspase-8 deficiency develop advanced neuroblastoma with bone marrow metastasis. Cancer Res 2013;73:4086–97.
11. Carter DR, Sutton SK, Pajic M, Murray J, Sekyere EO, Fletcher J, et al. Glutathione biosynthesis is upregulated at the initiation of MYCN-driven neuroblastoma tumorigenesis. Mol Oncol 2016;10:866–78.
12. Sun Y, Bell JL, Carter D, Gherardi S, Poulos RC, Milazzo G, et al. WDR5 supports an N-Myc transcriptional complex that drives a protumorigenic gene expression signature in neuroblastoma. Cancer Res 2015;75: 5143–54.
13. Carter DR, Murray J, Cheung BB, Gamble L, Koach J, Tsang J, et al. Therapeutic targeting of the MYC signal by inhibition of histone chaperone FACT in neuroblastoma. Sci Transl Med 2015;7:312ra176.
14. Esteller M. Non-coding RNAs in human disease. Nat Rev Genet 2011;12:861–74.
15. Esquela-Kerscher A, Slack FJ. Oncomirs - microRNAs with a role in cancer. Nat Rev Cancer 2006;6:259–69.
16. Swarbrick A, Woods SL, Shaw A, Balakrishnan A, Phua Y, Nguyen A, et al. miR-380-5p represses p53 to control cellular survival and is associated with poor outcome in MYCN-amplified neuroblastoma. Nat Med 2010;16:1134–40.
17. Lin RJ, Lin YC, Chen J, Kuo HH, Chen YY, Diccianni MB, et al. microRNA signature and expression of Dicer and Drosha can predict prognosis and delineate risk groups in neuroblastoma. Cancer Res 2010;70: 7841–50.
18. Das S, Bryan K, Buckley PG, Piskareva O, Bray IM, Foley N, et al. Modulation of neuroblastoma disease pathogenesis by an extensive network of epigenetically regulated microRNAs. Oncogene 2013;32:2927–36.
19. Mihailovich M, Bremang M, Spadotto V, Musiani D, Vitale E, Varano G, et al. miR-17-92 fine-tunes MYC expression and function to ensure optimal B cell lymphoma growth. Nat Commun 2015;6:8725.
20. Christoffersen NR, Shalgi R, Frankel LB, Leucci E, Lees M, Klausen M, et al. p53-independent upregulation of miR-34a during oncogene-induced senescence represses MYC. Cell Death Differ 2010;17:236–45.
21. Ritchie ME, Phipson B, Wu D, Hu Y, Law CW, Shi W, et al. limma powers differential expression analyses for RNA-sequencing and microarray studies. Nucleic Acids Res 2015;43:e47.
22. Mestdagh P, Van Vlierberghe P, De Weer A, Muth D, Westermann F, Speleman F, et al. A novel and universal method for microRNA RT-qPCR data normalization. Genome Biol 2009;10:R64.
23. De Preter K, Vandesompele J, Heimann P, Yigit N, Beckman S, Schramm A, et al. Human fetal neuroblast and neuroblastoma transcriptome analysis confirms neuroblast origin and highlights neuroblastoma candidate genes. Genome Biol 2006;7:R84.
24. Kocak H, Ackermann S, Hero B, Kahlert Y, Oberthuer A, Juraeva D, et al. Hox-C9 activates the intrinsic pathway of apoptosis and is associated with spontaneous regression in neuroblastoma. Cell Death Dis 2013;4:e586.
25. De Preter K, Mestdagh P, Vermeulen J, Zeka F, Naranjo A, Bray I, et al. miRNA expression profiling enables risk stratification in archived and fresh neuroblastoma tumor samples. Clin Cancer Res 2011;17:7684–92.
26. Liu B, Li J, Tsykin A, Liu L, Gaur AB, Goodall GJ. Exploring complex miRNA-mRNA interactions with Bayesian networks by splitting-averaging strategy. BMC Bioinformatics 2009;10:408.
27. Subramanian A, Tamayo P, Mootha VK, Mukherjee S, Ebert BL, Gillette MA, et al. Gene set enrichment analysis: a knowledge-based approach for interpreting genome-wide expression profiles. Proc Natl Acad Sci U S A 2005;102:15545–50.
28. Subramanian M, Li XL, Hara T, Lal A. A biochemical approach to identify direct microRNA targets. Methods Mol Biol 2015;1206:29–37.
29. Beckers A, Van Peer G, Carter DR, Mets E, Althoff K, Cheung BB, et al. MYCN-targeting miRNAs are predominantly downregulated during MYCNdriven neuroblastoma tumor formation. Oncotarget 2014;6: 5204–16.
30. Hogarty MD, Norris MD, Davis K, Liu X, Evageliou NF, Hayes CS, et al. ODC1 is a critical determinant of MYCN oncogenesis and a therapeutic target in neuroblastoma. Cancer Res 2008;68:9735–45.
31. Hsu CL, Chang HY, Chang JY, Hsu WM, Huang HC, Juan HF. Unveiling MYCN regulatory networks in neuroblastoma via integrative analysis of heterogeneous genomics data. Oncotarget 2016;7:36293–310.
32. Mogilyansky E, Rigoutsos I. The miR-17/92 cluster: a comprehensive update on its genomics, genetics, functions and increasingly important and numerous roles in health and disease. Cell Death Differ 2013; 20:1603–14.
33. Mestdagh P, Bostrom AK, Impens F, Fredlund E, Van Peer G, De Antonellis P, et al. The miR-17-92 microRNA cluster regulates multiple components of the TGF-beta pathway in neuroblastoma. Mol Cell 2010;40:762–73.
34. Shi L, Zhang B, Sun X, Lu S, Liu Z, Liu Y, et al. MiR-204 inhibits human NSCLC metastasis through suppression of NUAK1. Br J Cancer 2014;111: 2316–27.
35. Sacconi A, Biagioni F, Canu V, Mori F, Di Benedetto A, Lorenzon L, et al. miR-204 targets Bcl-2 expression and enhances responsiveness of gastric cancer. Cell Death Dis 2012;3:e423.
36. Ryan J, Tivnan A, Fay J, Bryan K, Meehan M, Creevey L, et al. MicroRNA-204 increases sensitivity of neuroblastoma cells to cisplatin and is associated with a favourable clinical outcome. Br J Cancer 2012;107:967–76.
37. Yin Y, Zhang B, Wang W, Fei B, Quan C, Zhang J, et al. miR-204-5p inhibits proliferation and invasion and enhances chemotherapeutic sensitivity of colorectal cancer cells by downregulating RAB22A. Clin Cancer Res 2014;20:6187–99.
38. Ding M, Lin B, Li T, Liu Y, Li Y, Zhou X, et al. A dual yet opposite growth-regulating function of miR-204 and its target XRN1 in prostate adenocarcinoma cells and neuroendocrine-like prostate cancer cells. Oncotarget 2015;6:7686–700.
39. Li T, Pan H, Li R. The dual regulatory role of miR-204 in cancer. Tumour Biol 2016;37:11667–77.

40. Beltran H, Rickman DS, Park K, Chae SS, Sboner A, MacDonald TY, et al. Molecular characterization of neuroendocrine prostate cancer and identification of new drug targets. Cancer Discov 2011;1:487–95.
41. Northcott PA, Buchhalter I, Morrissy AS, Hovestadt V, Weischenfeldt J, Ehrenberger T, et al. The whole-genome landscape of medulloblastoma subtypes. Nature 2017;547:311–7.
42. Corvetta D, Chayka O, Gherardi S, D'Acunto CW, Cantilena S, Valli E, et al. Physical interaction between MYCN oncogene and polycomb repressive complex 2 (PRC2) in neuroblastoma: functional and therapeutic implications. J Biol Chem 2013;288:8332–41.
43. Marshall GM, Gherardi S, Xu N, Neiron Z, Trahair T, Scarlett CJ, et al. Transcriptional upregulation of histone deacetylase 2 promotes Myc-induced oncogenic effects. Oncogene 2010;29:5957–68.
44. Liu T, Tee AE, Porro A, Smith SA, Dwarte T, Liu PY, et al. Activation of tissue transglutaminase transcription by histone deacetylase inhibition as a therapeutic approach for Myc oncogenesis. Proc Natl Acad Sci U S A 2007;104:18682–7.
45. Iraci N, Diolaiti D, Papa A, Porro A, Valli E, Gherardi S, et al. A SP1/MIZ1/MYCN repression complex recruits HDAC1 at the TRKA and p75NTR promoters and affects neuroblastoma malignancy by inhibiting the cell response to NGF. Cancer Res 2011;71:404–12.
46. Peter S, Bultinck J, Myant K, Jaenicke LA, Walz S, Muller J, et al. Tumor cell-specific inhibition of MYC function using small molecule inhibitors of the HUWE1 ubiquitin ligase. EMBO Mol Med 2014;6:1525–41.
47. Shahbazi J, Liu PY, Atmadibrata B, Bradner JE, Marshall GM, Lock RB, et al. The bromodomain inhibitor JQ1 and the histone deacetylase inhibitor panobinostat synergistically reduce N-Myc expression and induce anticancer effects. Clin Cancer Res 2016;22:2534–44.
48. Wee ZN, Li Z, Lee PL, Lee ST, Lim YP, Yu Q. EZH2-mediated inactivation of IFN-gamma-JAK-STAT1 signaling is an effective therapeutic target in MYC-driven prostate cancer. Cell Rep 2014;8:204–16.
49. Chipumuro E, Marco E, Christensen CL, Kwiatkowski N, Zhang T, Hatheway CM, et al. CDK7 inhibition suppresses super-enhancer-linked oncogenic transcription in MYCN-driven cancer. Cell 2014;159:1126–39.
50. Puissant A, Frumm SM, Alexe G, Bassil CF, Qi J, Chanthery YH, et al. Targeting MYCN in neuroblastoma by BET bromodomain inhibition. Cancer Discov 2013;3:308–23.
51. Otto T, Horn S, Brockmann M, Eilers U, Schuttrumpf L, Popov N, et al. Stabilization of N-Myc is a critical function of Aurora A in human neuroblastoma. Cancer Cell 2009;15:67–78.
52. Liu PY, Erriquez D, Marshall GM, Tee AE, Polly P, Wong M, et al. Effects of a novel long noncoding RNA, lncUSMycN, on N-Myc expression and neuroblastoma progression. J Natl Cancer Inst 2014;106. doi: 10.1093/jnci/dju113.
53. Gustafson WC, Meyerowitz JG, Nekritz EA, Chen J, Benes C, Charron E, et al. Drugging MYCN through an allosteric transition in Aurora kinase A. Cancer Cell 2014;26:414–27.
54. Brockmann M, Poon E, Berry T, Carstensen A, Deubzer HE, Rycak L, et al. Small molecule inhibitors of aurora-a induce proteasomal degradation of N-myc in childhood neuroblastoma. Cancer Cell 2013;24:75–89.